Shaped-Beam Luneburg Lens Antenna With Low Beam-Crossover Loss for 6G Communication

Xiaolian Mao, *Member, IEEE*, and Qiang Chen, *Senior Member, IEEE*

***Abstract*—Ensuring reliable, high-quality link coverage in 6G distributed communication systems requires favorable beam performance. This letter proposes a Luneburg-lens beam-shaping method and an antenna architecture based on pattern superposition to reduce beam-crossover loss (BCL). The architecture achieves 1.6× beamwidth broadening with overlapping dual-port excitation and a gain reduction of less than 1 dB. An 11-feed planar Luneburg lens prototype operating from 36 GHz to 40 GHz is designed for validation, with feeds spaced at 12° intervals. Compared with conventional single-feed operation, the shaped beam's peak gain decreases by 0.9 dB, and the BCL decreases from 6.5 dB to 2.3 dB, enabling an effective ±63° 3 dB beamwidth coverage range without increasing the number of feeds at 38 GHz. Due to its favorable beam performance, low complexity, low cost, and low power consumption, the proposed architecture is well-suited for large-scale deployment in 6G distributed communication systems.**

***Index Terms*—6G communication, beam-crossover loss, beam-shaping, Luneburg lens, millimeter-wave.**

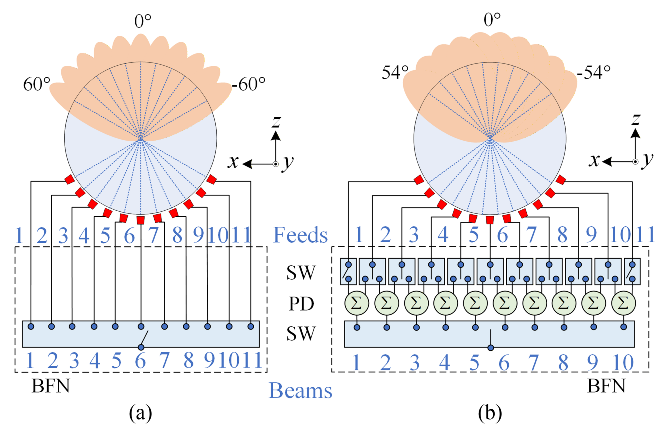

Fig. 1. Luneburg lens antenna architecture. (a) Conventional narrow beam with a ±60° scan range. (b) Proposed shaped beam with a ±54° scan range. (SW: switch; PD: power divider; BFN: beamforming network.)

I. Introduction

Future 6G distributed communication systems aim to provide uniform quality of service by spatially and functionally distributing antennas, radio units, and computing resources across macro sites, small cells, and edge clouds, particularly in dense urban, industrial, and hotspot scenarios, operating in the millimeter-wave and terahertz bands. Within this system-level paradigm, cell-free massive multiple-input–multiple-output (MIMO) has emerged as a key radio access architecture. However, the large-scale deployment of such cell-free architectures at high frequencies is fundamentally constrained by the cost and power consumption of dense RF front-ends at distributed access points (APs). Lens antennas, owing to their favorable multibeam characteristics, low cost, and low power consumption, have been extensively studied. [1], [2], [3], [4], [5], [6], [7], [8], [9], [10] report Luneburg lens-based multibeam antennas with single-feed switching, where each beam is high-gain but narrow, leading to high beam crossover loss (BCL). A central issue in multibeam antennas is BCL, which directly affects coverage continuity and link efficiency. For reliable, high-quality link coverage, both low BCL and a wide-angle 3 dB beamwidth coverage range (BCR) are essential [11].

Received 24 April 2026; accepted 20 May 2026. Date of publication 22 May 2026; date of current version 9 July 2026. This work was supported in part by JST SPRING under Grant JPMJSP2114 and in part by the STEP-ALICE Program at Tohoku University. *(Corresponding author: Xiaolian Mao.)*

The authors are with the Department of Communications Engineering, Tohoku University, Sendai 980-8579, Japan (e-mail: mao.xiaolian.r2@dc.tohoku.ac.jp; qiang.chen.a5@tohoku.ac.jp).

Digital Object Identifier 10.1109/LAWP.2026.3696085

In Zetterstrom et al. [12], a generalized Luneburg lens improves angular resolution of feed placement by displacing the focal arc from the lens boundary, achieving a BCL of 2 dB to 4 dB and relatively high aperture efficiency. However, the design requires many feeds, and edge-feed shading significantly limits its ability to achieve a wide-angle 3 dB BCR. [13] reports fully metallic partial Maxwell fish-eye (PMFE) lens arrays, and [14] reports a small-scale array-fed gradient-index (GRIN) lens. Both approaches can achieve a BCL below 3 dB with a wide-angle BCR, but they require phase-controlled feeding networks that increase structural complexity and cost. Su and Chen [15] and Xu and Chen [16] report transformation-optics metamaterial-based Luneburg lenses with linear feed alignment; Yin et al. [17] report a multipoint pillbox source combined with an overlaid metasurface lens; and Zetterström et al. [18] report a virtual image lens with a non-collimated broad beam. These approaches can achieve a low BCL, but the 3 dB BCR remains limited. In lens-based multibeam systems, adjacent-port joint excitation or weighted excitation is often used to improve beam coverage performance [19]. Lian et al. [20] report a Rotman-lens substrate-integrated waveguide (SIW) array that uses dual-port excitation to improve isolation and cross-polarization performance between the two sub-lenses. Lian et al. [21] report a Rotman-lens SIW array that uses dual-port excitation to reduce the sidelobe level. In Cao et al. [22], a Rotman-lens SIW array uses dual-source excitation to achieve a low BCL and sidelobe level. However, the Rotman lens is inherently a passive true-time-delay beamforming network for array feeding; it struggles to achieve a wide-angle 3 dB BCR, and its aperture efficiency is typically limited.

Overall, no dedicated study has yet been reported on a Luneburg lens-based multifeed beam-shaping antenna system. In the proposed design, overlapping dual-port excitation is applied to a planar Luneburg lens to synthesize shaped beams via pattern superposition, thereby achieving both low BCL and a wide-angle 3 dB BCR. Compared with existing approaches, the proposed method offers a practical trade-off among feed-network complexity, aperture efficiency, and beam coverage performance. To validate this concept, we fabricated a 3-D-printed planar Luneburg lens prototype operating at 36 GHz to 40 GHz. The prototype uses 11 printed dipole feeds with 12° angular spacing to generate 10 shaped beams, achieving about 1.6× beamwidth broadening, BCL below 3 dB, and an overall 3 dB BCR of ±60° across 36 GHz to 40 GHz.

II. Antenna Design

A. Beam-Shaping Method and Antenna Architecture

The Luneburg lens relies on a radially GRIN profile such that an ideal point source placed on the lens rim produces a quasi-plane wave after transmission through the lens. The refractive-index distribution is [23]

$$n(r) = \sqrt{2 - (r/R)^2},\ 0 \le r \le R \tag{1}$$

where r is the radial distance to the lens center, and R is the lens radius. In practical implementations, the feed has a finite physical aperture, rather than an ideal point source. The effective radiating aperture of the feed strongly impacts the formed beam's gain and width. Leveraging this property, beam shaping can be achieved by adjusting the feed aperture. In this work, we implement this adjustment by simultaneously exciting multiple feeds to control the effective aperture at the lens's rim. Unlike linear or arc arrays, where an element-spacing-dependent array factor dominates beam shaping, a Luneburg lens excited by multiple feeds exhibits pattern superposition. The total far field is

$$\mathrm{E}_{\text{tot}}(\theta,\phi) = \sum_{m=1}^{M} w_m \mathrm{E}_m(\theta,\phi),\ w_m = a_m e^{j\psi_m} \tag{2}$$

where $\mathrm{E}_m(\theta,\phi)$ is the complex far field when only the mth feed is excited with unit power, w_m is the complex weight, a_m and ψ_m are the amplitude and phase weights, M is the number of simultaneously active feeds. By judiciously choosing w_m, the Luneburg lens can synthesize shaped beams as required. However, when multiple feeds are excited simultaneously, the peak gain can drop significantly compared with conventional single-feed operation. To minimize gain degradation while keeping the beamforming network as simple as possible, we propose a Luneburg-lens antenna architecture that excites only two adjacent feeds at a time and uses overlapping dual-port excitation to synthesize the shaped beam and reduce BCL.

Using a three-feed case as an example, consider two adjacent feeds excited with equal amplitude and phase. If the corresponding single-feed patterns are approximately identical and their overlap-region phases are nearly aligned, then, on the principal *H*-plane cut, the single-feed power pattern can be approximated by a Gaussian beam [24] with a 3 dB beamwidth $BW_1(f)$. Assuming the synthesized shaped beam pattern remains single-peaked with a 3 dB beamwidth $BW_{12}(f)$. The angular spacing between adjacent single-feed beam peaks is $\Delta\theta$, which, for a Luneburg lens, can be approximated by the angular spacing between adjacent feeds. Therefore, the intersection angle of the two shaped beams is approximately aligned with the shared feed 2. Then the shaped-beam BCL can be approximately written as [19], [25]

$$\text{BCL}(f) \approx 3.01(\Delta\theta / BW_{12}(f))^2,\ BW_{12}(f) \approx K_b BW_1(f) \tag{3}$$

where K_b is the beam-broadening factor, f is in GHz, and BCL is in dB. Thus, when $\Delta\theta$ is fixed, as frequency increases, both the original narrow beams and the shaped beams become narrower, the overlap between adjacent beams decreases, and the BCL increases.

The proposed shaped-beam lens antenna architecture, as shown in Fig. 1, requires only one additional set of power dividers and a switch matrix, compared with conventional Luneburg-lens designs and existing beam-shaping methods, without adding extra attenuators, phase shifters, or feed elements. Therefore, it maintains relatively low structural complexity and power consumption. With 11 feeds arranged at 12° intervals, 10 shaped beams are formed, providing a beam scanning range (BSR) of ±54° and an overall 3 dB BCR exceeding ±60°. To validate the proposed method and antenna architecture, we designed a planar Luneburg lens antenna with 11 printed-dipole feeds. The proposed method is also applicable to 3-D Luneburg lenses.

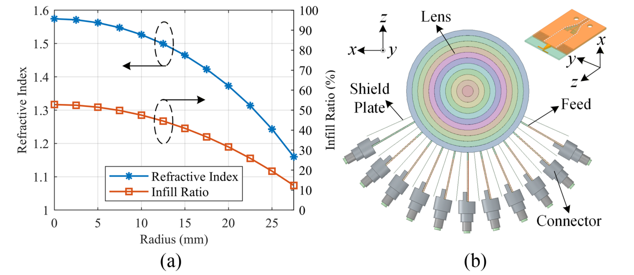

Fig. 2. (a) Refractive-index and infill-ratio distributions versus the radius of the proposed lens. (b) Configuration of the proposed planar Luneburg lens antenna with printed dipole feeds.

B. Prototype Design and Analysis

A multilayer dielectric planar Luneburg lens prototype is designed with a total thickness of 9 mm and a radius of 27.5 mm. Radially, the lens is divided into 11 concentric annular layers, each 2.5 mm wide. The refractive-index distribution is modified to range from 1.57 to 1.16 [6]. By controlling the polylactic acid (PLA) infill ratio from 82% to 19% during 3-D printing [26], [27], a multilayer dielectric lens can be realized without a complex structural design. The distributions of the lens refractive index and infill ratio are shown in Fig. 2(a). During beam shaping, beam broadening inevitably reduces gain and aperture efficiency. Therefore, it is crucial to design a feed that closely approximates an ideal point source. As shown in Fig. 2(b), a printed dipole feed based on a grounded coplanar waveguide (GCPW)-SIW transition [28], [29] is designed. It uses a low-loss Rogers RT/duroid 5880 substrate ($\varepsilon_r = 2.2$, $\tan\delta = 0.0009$) with a thickness of 0.508 mm.

The overall lens antenna setup is shown in Fig. 2(b). It includes a multilayer dielectric lens, 11 printed dipole feeds with arms aligned along the *y*-axis, and copper shielding plates between adjacent feeds to reduce mutual coupling. Full-wave simulations

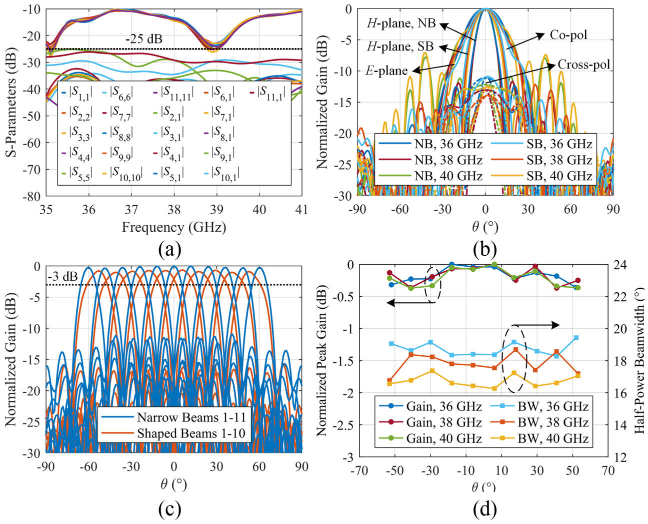

Fig. 3. (a) Simulated S-parameters of the lens antenna's feed ports. (b) Simulated radiation patterns for Beam 6 at 36 GHz, 38 GHz, and 40 GHz. (c) Simulated radiation patterns for all beams in the H-plane at 38 GHz. The shaped beams are normalized to the peak gain of the narrow beams. (d) Normalized peak gain and HPBW for 10 shaped beams. (NB: narrow beam; SB: shaped beam; Co-pol (solid): copolarization; Cross-pol (dashed): cross-polarization; BW: beamwidth.)

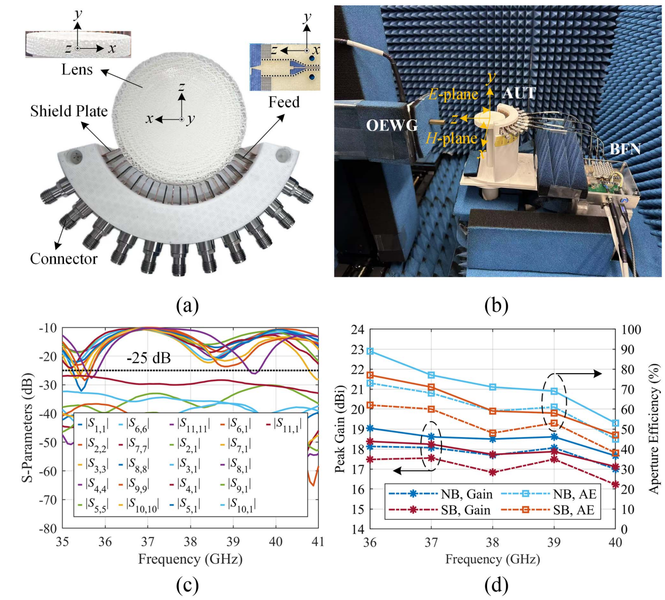

Fig. 4. (a) Photographs of the fabricated planar Luneburg lens with feeds. (b) Measurement setup. (c) Measured *S*-parameters of the lens antenna's feed ports. (d) Measured (dashed) and simulated (solid) peak gain and aperture efficiency for Beam 6 over 36 GHz to 40 GHz. (OEWG: open-ended waveguide; AUT: antenna under test; AE: aperture efficiency.)

are performed using HFSS. The reflection and mutual coupling coefficients for all ports are below −10 dB and −25 dB, respectively, as shown in Fig. 3(a). The radiation patterns of the narrow and shaped beams at 36 GHz, 38 GHz, and 40 GHz are shown in Fig. 3(b). At low, middle, and high frequencies, the *H*-plane radiation pattern broadens significantly, whereas the *E*-plane pattern remains nearly unchanged. Fig. 3(d) shows the normalized peak gain and half-power beamwidth (HPBW) for 10 shaped beams. Fig. 6(a) shows the envelopes, normalized to the peak gain of the narrow beams at 36 GHz, 38 GHz, and 40 GHz. As shown in Fig. 6(b), the simulated BCLs for the narrow beams were 4.2 dB, 4.1 dB, and 4.1 dB, respectively. These values were insufficient to sustain a 3 dB BCR over ±60°. In contrast, the shaped beams achieved BCLs of 1.5 dB, 1.7 dB, and 2.3 dB, with peak-gain reductions of only 0.6 dB, 0.9 dB, and 0.6 dB relative to the narrow-beam mode, enabling a 3 dB BCR over ±60°. As frequency increases, the shaped beams become narrower, the flatness of the envelopes decreases, and the BCL increases.

III. Fabrication, Measurement, and Discussion

A. Antenna Fabrication

The proposed planar Luneburg lens was fabricated on an UltiMaker S5 3D printer using PLA ($\varepsilon_r \approx 2.8$) [13] with a gyroid infill pattern. The lens was printed monolithically by setting local infill densities to match the designed index profile. The printed dipole feed was fabricated using a standard PCB process on a Rogers RT/duroid 5880 substrate. The antenna bracket was also fabricated on the 3-D printer to mechanically integrate the lens and feeds. Shielding plates made of 0.3 mm thick copper sheets were installed between adjacent feeds. Fig. 4(a) shows the fabricated hardware.

TABLE I
Comparison of Measured and Simulated Radiation Pattern Parameters at 38 GHz

Parameter	Gain (dBi)	HPBW (°) *H/E*	Cross-pol (dB)	SLL (dB) *H*	BCL (dB) *H*	BSL (dB) *H*
Beam	6	6	6	All	All	All
Sim. NB	18.5	10.7 /23.8	−13	−11	4.1	0.4
Meas. NB	17.7	9.9/ 24.1	−16	−10	6.5	0.9
Sim. SB	17.6	17.5 / 21.6	−14	−15	1.7	0.4
Meas. SB	16.8	17.3/ 23.6	−15	−12	2.3	1.1

Note: *H/E* = *H*-plane/*E*-plane; SLL = sidelobe level; BSL = beam scan loss; Sim. = simulation; Meas. = measurement.

B. Measurement and Results

As shown in Fig. 4(b), measurements were performed in a near-field anechoic chamber. First, a vector network analyzer (Agilent N5224A) was used to measure the *S*-parameters of all 11 ports. Second, a TMYTE BBoard 5G 39 GHz beamformer was used as BFN for channel calibration and beam emulation. The beamformer provides four RF channels with independent amplitude and phase control, with 0.5 dB and 5.625° steps, respectively. The 11 narrow beams and 10 shaped beams were obtained over four sequential measurement passes.

Table I summarizes the key parameters of the measured and simulated patterns. Fig. 4(c) shows that the measured feed-port reflection and mutual coupling coefficients are below −10 dB and −25 dB, respectively, across 36 GHz to 40 GHz. Fig. 4(d) shows the peak gain and aperture efficiency. Over 36 GHz to 40 GHz, the measured peak gain of Beam 6 is 17.0 dBi to 18.1 dBi (narrow beams) and 16.2 dBi to 17.5 dBi (shaped beams); the measured aperture efficiency is 45%–73% (narrow beams) and 38%–62% (shaped beams). Fig. 5(a) compares

TABLE II
COMPARISON WITH REPORTED LENS ANTENNA

Ref.	Realization	Freq. (GHz)	Peak Gain (dBi)	HPBW (°) *H*	BSR (°) *H*	3-dB BCR (°) *H*	BCL (dB) *H*	BSL (dB) *H*	SLL (dB) *H*	AE
[3]	Fully metallic stacked Luneburg lens with 13 WG feeds.	60	22.5	6	±55	n.a	>5.0	1.0	–10	40%
[4]	PCB-stacked Luneburg lens with 11 printed feeds.	29	15.4	10	±72	n.a	>5.0	n.a	n.a	42%
[12]	Fully metallic Luneburg lens with 21 RWG feeds placed by displacing the focal arc from the lens boundary.	62	18.5	n.a	±51	≈ ±53	3.0	n.a	–10	90% (Sim.)
[13]	Fully metallic PMFE lens array with WG feeder array and phase-shifting networks.	28	20.3	10.5	±65.5	±70.8	3.0	5.6	–8	21–76%
[14]	3D-printed gradient-index lens with patch-array feeds.	28	28.2	10	±58	±63	3.0	3.1	–13	33–68%
[22]	Rotman Lens SIW array with dual-source excitation.	5.8	22.3	n.a	±50	≈ ±55	2.6	2.1	-13	30–45%
This work	3D printing Luneburg lens with 11 printed dipole feeds and overlapping dual-port excitation	38	16.8	17	±54	±63	2.3	1.1	–12	39–48%

Note: Ref. = reference; Freq. = frequency; WG = waveguide; RWG = ridge waveguide; n.a. = not available.

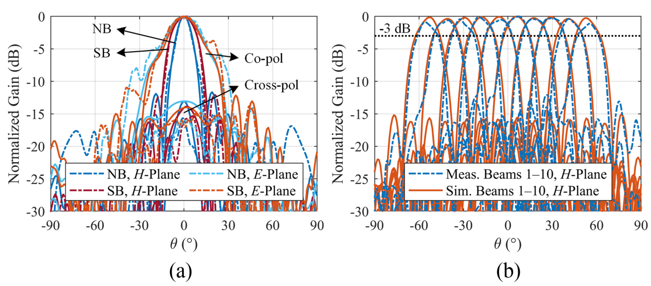

Fig. 5. Measured (dashed) and simulated (solid) normalized radiation patterns at 38 GHz. (a) Beam 6 in the *H*- and *E*-planes. (b) All shaped beams in the *H*-plane.

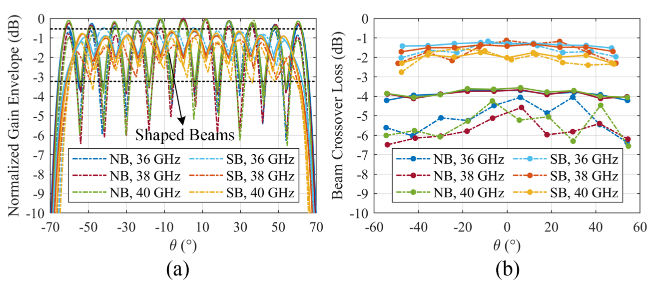

Fig. 6. Measured (dashed) and simulated (solid). (a) Normalized radiation pattern envelopes. (b) BCLs in the *H*-plane. The envelopes are normalized to the peak gain of the narrow beams at each frequency.

narrow and shaped beams at 38 GHz by showing their radiation patterns, while Fig. 5(b) shows the *H*-plane patterns for all shaped beams. The measured SLL is below −12 dB. Fig. 6(a) and (b) present the measured normalized radiation pattern envelopes and BCLs in the *H*-plane at 36 GHz, 38 GHz, and 40 GHz. The narrow beams achieve measured BCLs of 6.4 dB, 6.5 dB, and 6.6 dB. In contrast, the shaped beams achieve BCLs of 2.0 dB, 2.3 dB, and 2.8 dB, respectively, with peak-gain reductions of 0.5 dB, 0.9 dB, and 1.0 dB relative to the narrow-beam mode, enabling 3 dB BCRs over ±60°. Compared with the simulated BCLs, the differences are 0.5 dB, 0.6 dB, and 0.5 dB, respectively. The measurements follow the same frequency-dependent trend as the simulations, with slight degradation.

C. Discussion and Comparison

The measured results agree well with the simulated results, validating the feasibility of the proposed beam-shaping method and lens antenna architecture. The results show that the proposed design maintains stable performance across 36 GHz to 40 GHz. The differences in gain, SLL, and BCL are primarily due to fabrication tolerances, feed assembly errors, channel amplitude and phase errors, and measurement positioning errors. The *H*-plane patterns agree well with the simulations, whereas larger deviations in some beams are mainly due to accumulated beam-pointing errors. The discrepancy in SLL is also influenced by the structural effects of the antenna bracket and the measurement fixture, which can introduce additional scattering. The *E*-plane distortion near ±20° and the increased SLLs are mainly attributed to the low infill density of the outermost 3-D-printed lens layer, as shown in Fig. 4(a).

Table II compares this work with the reported Lens Antenna. In summary, compared with conventional single-feed-switching Luneburg lenses [4], [5], the proposed design significantly improves the BCL. Compared with the optimized-feed-arrangement scheme in Zetterstrom et al. [12] and the Rotman-lens-fed architecture in Cao et al. [22], it provides a wider BCR while maintaining a simpler, lower-cost feeding structure than the phase-controlled solutions in Nie et al. [13] and Qu et al. [14]. Therefore, the proposed method and antenna architecture offer an effective way to reduce the BCL of multi-beam Luneburg-lens antennas and achieve a wide-angle 3 dB BCR.

IV. CONCLUSION

This letter presents a beam-shaping method and an antenna architecture based on a Luneburg lens. A prototype planar Luneburg lens with 11 feeds spaced at 12° intervals was fabricated and experimentally validated, demonstrating good performance. With overlapping dual-port excitation, 10-shaped broad beams are formed, providing an overall 3 dB BCR of ±60° across 36 GHz to 40 GHz, with a gain reduction relative to the narrow beam of less than 1 dB. Benefiting from its favorable beam performance, low hardware complexity, low cost, and low power consumption, the proposed architecture meets the diverse deployment requirements of 6G distributed communication systems.

REFERENCES

[1] Y. Li, L. Ge, M. Chen, Z. Zhang, Z. Li, and J. Wang, "Multi-beam 3-D-printed luneburg lens fed by magnetoelectric dipole antennas for millimeter-wave MIMO applications," *IEEE Trans. Antennas Propag.*, vol. 67, no. 5, pp. 2923–2933, May 2019, doi: 10.1109/TAP.2019.2899013.

[2] C. Wang, J. Wu, and Y.-X. Guo, "A 3-D-printed multibeam dual circularly polarized Luneburg lens antenna based on quasi-icosahedron models for Ka-band wireless applications," *IEEE Trans. Antennas Propag.*, vol. 68, no. 8, pp. 5807–5815, Aug. 2020, doi: 10.1109/TAP.2020.2983798.

[3] P. Castillo-Tapia et al., "Two-dimensional beam steering using a stacked modulated geodesic luneburg lens array antenna for 5G and beyond," *IEEE Trans. Antennas Propag.*, vol. 71, no. 1, pp. 487–496, Jan. 2023, doi: 10.1109/TAP.2022.3217175.

[4] X. Wang, Y. Cheng, and Y. Dong, "A wideband PCB-stacked air-filled Luneburg lens antenna for 5G millimeter-wave applications," *IEEE Antennas Wireless Propag. Lett.*, vol. 20, no. 3, pp. 327–331, Mar. 2021, doi: 10.1109/LAWP.2021.3049432.

[5] O. Quevedo-Teruel, J. Miao, M. Mattsson, A. Algaba-Brazalez, M. Johansson, and L. Manholm, "Glide-symmetric fully metallic Luneburg lens for 5G communications at Ka-band," *IEEE Antennas Wireless Propag. Lett.*, vol. 17, no. 9, pp. 1588–1592, Sep. 2018, doi: 10.1109/LAWP.2018.2856371.

[6] X. Mao and Q. Chen, "Hybrid beam-switching and scanning millimeter-wave array with planar Luneburg lenses," *IEEE Antennas Wireless Propag. Lett.*, vol. 25, no. 2, pp. 531–535, Feb. 2026, doi: 10.1109/LAWP.2025.3631510.

[7] Z. Wang et al., "A wideband dual-circularly polarized luneburg lens multibeam antenna fed by dual-linearly polarized ME-dipole antennas," *IEEE Antennas Wireless Propag. Lett.*, vol. 73, no. 5, pp. 2804–2813, May 2025, doi: 10.1109/TAP.2024.3523634.

[8] H. Li, M. Li, H. Lu, and W. Yu, "Experimental realization of 140 GHz metallic lens antenna with designable multiple beams," *IEEE Antennas Wireless Propag. Lett.*, vol. 24, no. 11, pp. 4373–4377, Nov. 2025, doi: 10.1109/LAWP.2025.3567631.

[9] B. Nie, Y. Liu, H. Lu, Y. Gao, Y. Wang, and S. Gao, "Fully metallic dual-band-multibeam aperture-shared lens antenna for N257 millimeter-wave and N79 sub-6 GHz applications," *IEEE Trans. Antennas Propag.*, vol. 73, no. 10, pp. 7303–7313, Oct. 2025, doi: 10.1109/TAP.2025.3580278.

[10] T. Ao and Y. Dong, "Millimeter-wave dual-polarized Luneburg lens antenna based on hybrid dual-mode unit cell," *IEEE Trans. Antennas Propag.*, vol. 73, no. 12, pp. 10803–10808, Dec. 2025, doi: 10.1109/TAP.2025.3597018.

[11] O. Zetterstrom, J. Rico-Fernández, J. L. Gómez-Tornero, and A. Algaba-Brazález, "Industrial evolution of lens antennas toward 6G radio access applications," *IEEE Antennas Wireless Propag. Lett.*, vol. 23, no. 11, pp. 3594–3598, Nov. 2024, doi: 10.1109/LAWP.2024.3365882.

[12] O. Zetterstrom et al., "V-band geodesic generalized luneburg lens antenna with high beam crossover gain," *IEEE Antennas Wireless Propag. Lett.*, vol. 71, no. 9, pp. 7591–7596, Sep. 2023, doi: 10.1109/TAP.2023.3283138.

[13] B. Nie, Y. Liu, H. Lu, Z. Liu, Y. Gao, and P. Zhen, "Fully metallic gradient index lens array antenna for wide-angle scanning phased array," *IEEE Trans. Antennas Propag.*, vol. 71, no. 9, pp. 7363–7375, Sep. 2023, doi: 10.1109/TAP.2023.3296198.

[14] Z. Qu, S.-W. Qu, Z. Zhang, S. Yang, and C. H. Chan, "Wide-angle scanning lens fed by small-scale antenna array for 5G in millimeter-wave band," *IEEE Trans. Antennas Propag.*, vol. 68, no. 5, pp. 3635–3643, May 2020, doi: 10.1109/TAP.2020.2967086.

[15] Y. Su and Z. N. Chen, "A flat dual-polarized transformation-optics beam-scanning Luneburg lens antenna using PCB-stacked gradient index metamaterials," *IEEE Trans. Antennas Propag.*, vol. 66, no. 10, pp. 5088–5097, Oct. 2018, doi: 10.1109/TAP.2018.2858209.

[16] R. Xu and Z. N. Chen, "A hemispherical wide-angle beamsteering near-surface focal-plane metamaterial luneburg lens antenna using transformation-optics," *IEEE Trans. Antennas Propag.*, vol. 70, no. 6, pp. 4224–4233, Jun. 2022, doi: 10.1109/TAP.2021.3138554.

[17] S.-Y. Yin, J.-L. Li, Y.-M. Zhang, and Q.-C. Ye, "Fan-shaped multi-beam metasurface lens antenna for high crossover levels and stable radiation gain," *IEEE Antennas Wireless Propag. Lett.*, vol. 23, no. 6, pp. 1809–1813, Jun. 2024, doi: 10.1109/LAWP.2024.3370262.

[18] O. Zetterstrom, N. J. G. Fonseca, and O. Quevedo-Teruel, "Wide-angle beam-switching antenna with stable gain based on a virtual image lens," *Electronics*, vol. 13, no. 6, Mar. 2024, Art. no. 1034, doi: 10.3390/electronics13061034.

[19] J. L. Volakis, Ed., *Antenna Engineering Handbook*, 4th ed. New York, NY, USA: McGraw-Hill, 2007.

[20] J.-W. Lian, H.-N. Wu, C. Geng, W. Hong, and D. Ding, "Compact millimeter-wave orthogonal SIW multibeam antenna based on shared-cavity Rotman lens and shared-aperture array antenna," *IEEE Trans. Antennas Propag.*, vol. 73, no. 8, pp. 6169–6174, Aug. 2025, doi: 10.1109/TAP.2025.3564737.

[21] J.-W. Lian, Y.-L. Ban, H. Zhu, and Y. J. Guo, "Reduced-sidelobe multibeam array antenna based on SIW Rotman lens," *IEEE Antennas Wireless Propag. Lett.*, vol. 19, no. 1, pp. 188–192, Jan. 2020, doi: 10.1109/LAWP.2019.2957509.

[22] Y. Cao, S. Wu, J. Zhang, J. Li, and S. Yan, "Compact 2-D passive beam-scanning multibeam antenna based on Rotman lens and mechanical sweeping phase gradient metasurface," *IEEE Trans. Antennas Propag.*, vol. 73, no. 7, pp. 4993–4998, Jul. 2025, doi: 10.1109/TAP.2025.3553748.

[23] R. K. Luneburg, *Mathematical Theory of Optics*. Berkeley, CA, USA: Univ. California Press, 1964.

[24] C. A. Balanis, Ed., *Modern Antenna Handbook*. Hoboken, NJ, USA: Wiley, 2008.

[25] R. J. Mailloux, *Phased Array Antenna Handbook*, 2nd ed. Norwood, MA, USA: Artech House, 2005.

[26] S. Zhang, R. K. Arya, S. Pandey, Y. Vardaxoglou, W. Whittow, and R. Mittra, "3D-printed planar graded index lenses," *Microw., Antennas Propag.*, vol. 10, no. 13, pp. 1411–1419, 2016.

[27] I. Kuzmanić, I. Vujović, M. Petković, and J. Šoda, "Influence of 3D printing properties on relative dielectric constant in PLA and ABS materials," *Prog. Addit. Manuf.*, vol. 8, pp. 703–710, Feb. 2023, doi: 10.1007/s40964-023-00411-0.

[28] F. F. Manzillo, M. Ettore, M. S. Lahti, K. T. Kautio, D. Lelaidier, and E. Seguenot, "A multilayer LTCC solution for integrating 5G access point antenna modules," *IEEE Trans. Microw. Theory Techn.*, vol. 64, no. 7, pp. 2272–2283, Jul. 2016, doi: 10.1109/TMTT.2016.2574313.

[29] Z. Zhang, K. Wu, and N. Yang, "Broadband millimeter-wave quasi-Yagi antenna using substrate integrated waveguide technique," in *Proc. IEEE Radio Wireless Symp.*, Orlando, FL, USA, 2008, pp. 671–674, doi: 10.1109/RWS.2008.4463581.